

# Electrostatic Tractor Analysis Using a Measured Flux Model

Joseph Hughes and Hanspeter Schaub

**Abstract**—Although spacecraft charging is often thought of as a purely harmful phenomena, if controlled it can be used as a means of touchless actuation. If a tug spacecraft irradiates a debris object with an electron beam, the tug will charge positive and the debris will charge negative. There will then be an attractive Coulomb force that the tug can use to tug the debris object from geosynchronous orbit into a graveyard orbit. Compared to earlier work this paper uses a more advanced charging model with isotropic fluxes for the calculation of electron and ion-induced yields, and an empirical model of electron and ion fluxes rather than Maxwellian distributions. This new model is used to calculate the attractive force for a variety of tug to debris size ratios, beam currents and voltages, and the inclusion of pulsing the electron beam. The major result of using this new charging model is that it takes more current than was used in prior work to charge a debris object due to the higher yields from isotropic fluxes. Despite this, the ET concept can easily move a range of debris objects to the graveyard orbit in a few months.

**Index Terms**—Electrostatic Tractor; Orbital Debris; Re-Orbiting

## I. INTRODUCTION

Spacecraft charging is often thought of as a harmful phenomena that must be prevented or mitigated to insure mission success. However, if controlled, it can have beneficial effects that enable new and exciting missions. For instance, a number of concepts have been proposed to purposely charge a spacecraft so that is pushed by the Earth’s magnetic field through the Lorentz field to change its orbit without expending fuel [1, 2, 3]. Another family of concepts use the Coulomb force between a pair of charged spacecraft rather than the interaction with the Earth’s magnetic field to exert touchless forces and torques.

If a servicing vehicle irradiates a passive conducting space object with an electron beam the servicer charges positive and the passive craft charges negative resulting in an attractive Coulomb force between them. This force can be used for small orbital corrections in a formation flying mission with negligible use of propellant [4, 5, 6, 7]. If the charge distribution on the passive craft is not evenly distributed about the center of mass, the passive craft will also experience an electrostatic torque [8, 9, 10]. The concept has broad applicability with propellant-free formation flying and touchless de-spin before docking or servicing. One special case of this concept is the called the Electrostatic Tractor (ET) shown in Fig. 1 where a tug craft

pulls a piece of space debris from geosynchronous (GEO) orbit into a graveyard orbit 200-300 km higher than GEO [11, 12]. Moving GEO debris from active belt is important to prevent satellite collisions which could easily cause more collisions and destroy every satellite in GEO in what is known as the “Kessler” Syndrome [13]. Although much orbital debris research focuses on the Low Earth Orbit (LEO) regime, Oltrogge shows that the spatial densities in GEO can be as high as those in LEO [14]. Anderson [15, 16] determines that given the imperfect mitigation efforts, the number of near-miss events near gravitational wells will double in 50 years. Multiple studies conclude that mitigation measures must be combined with active debris removal (ADR) to ensure the long-term safety and usability of the GEO ring [17, 18, 19, 20].

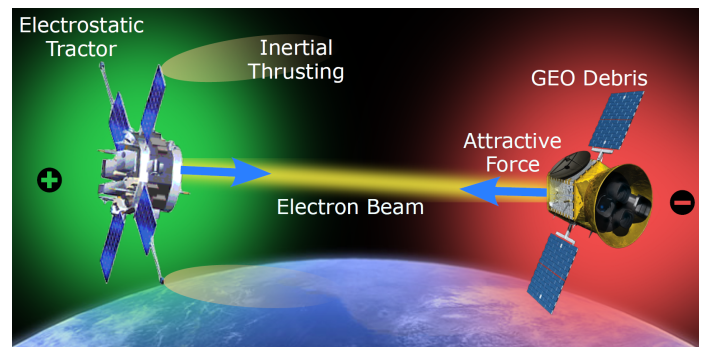


Fig. 1: Concept of operations for the Electrostatic Tractor

This paper analyzes the ET concept with a higher-fidelity charging model than has been used before. The first analysis of the charging aspect of the ET [21] included electron and ion thermal currents using a nominal Maxwellian current model, the photoelectric current, and Secondary Electron Emission (SEE) from the beam electrons, but neglected SEE and backscattering from the thermal currents. Hogan and Schaub in [22] further develop the ET charging model by considering the Maxwellian thermal currents at planetary K-indices of  $K_P = 1.5$  and 6. Additionally, they account for SEE and photoelectrons from the debris that provide an additional negative current to the tug. Reference [23] also investigates the performance of the ET with normal variations in the plasma parameters throughout an orbit using single Maxwellian populations based on work by Denton et. al. [24]. More force is produced in the early morning sector (Local Times between 1 and 6) due to the high temperature electron plasma in that region. Reference [25] investigates a pulsed electron beam with the same Maxwellian-based model as [22] but solve the equations with respect to time to account for the

Joseph Hughes is a graduate research assistant at the University of Colorado at Boulder, (email: Joseph.Hughes@Colorado.edu)

Hanspeter Schaub is a Professor and Glenn L. Murphy Chair of Engineering at the University of Colorado at Boulder, (email: Hanspeter.Schaub@Colorado.edu)

charge-up and discharging behavior. Reference [26] uses the same model as [23] for a changing single Maxwellian model of the plasma variations throughout an orbit.

This paper does not use Maxwellian currents at all but rather uses an empirical model [27] to predict the flux as a function of energy, local time ( $LT$ ) and Planetary K index ( $K_P$ ). This flux distribution is numerically integrated to give the current to the spacecraft as well as the SEE and backscattering yield at a given spacecraft potential. Additionally, all yields except that from the electron beam are assumed to be isotropic as opposed to prior work which used normal incidence. Once the charging model is developed, the ET force is studied for candidate mission scenarios for multiple beam currents and voltages as a function of local time for both a calm space weather condition ( $K_P = 2-$ ) and a stormy space weather condition ( $K_P = 8$ ). Then, the optimal orbit-averaged forces are investigated for many different power and tug-to-debris size levels. Next, pulsing is re-examined for long pulse periods as a function of power and size ratios.

## II. THE SPACE ENVIRONMENT

In early analysis of charging for the ET, [21, 22, 23], electrons were modeled by a single Maxwellian with  $n_E \sim 1 \text{ cm}^{-3}$  and  $kT_E \sim 1 \text{ keV}$  and ions by a single Maxwellian with  $n_I \sim 1 \text{ cm}^{-3}$  and  $kT_I \sim 50 \text{ eV}$ . In contrast, the spacecraft charging community often uses much hotter distributions for both ions and electrons with temperatures in the 10s of keV for electrons and near 30 keV for ions [28]. This work introduces a third model of the GEO space environment.

Denton et. al. [27] present an empirical model that uses 82 satellite-years of observed electron and ion flux data. Both populations are measured by Magnetospheric Plasma Analyzers (MPAs) on board multiple Los Alamos National Labs (LANL) satellites. The MPAs are capable of measuring the flux between 1 eV and 40 keV in three spatial dimensions every 86 seconds. All of this data is tagged with local time ( $LT$ ),  $K_P$  index, and solar wind electric field ( $vB_z$ ), which allows interpolation on a variety of cases. The model allows users to specify three inputs (Energy,  $LT$ , and  $K_P$  or  $vB_z$ ) and outputs the mean, median, and percentile flux values. This work considers a calm case where  $K_P = 2-$  and a severe storm with  $K_P = 8$ . Because the flux is only measured between 1 eV and 40 keV, it is not a complete picture of the environment since there is flux at both higher and lower energies. Also, the measured electron flux at low energies is a combination of the natural space environment and the secondary and photoelectrons generated by the spacecraft itself. Additionally, because the spacecraft is sometimes negative, it will turn away environmental electrons with less energy than the spacecraft's voltage. These two effects both obscure the true environmental electrons below  $\sim 100 \text{ eV}$ . These contaminations of the electron data and the missing data above 40 keV and below 1 eV are sources of error. For instance, the total density of electrons in the late night sector at  $K_P = 2-$  is slightly less than  $1 \text{ cm}^{-3}$ , but the ion density is between 2 and  $4 \text{ cm}^{-3}$ . If this were true it would seriously violate the principle of quasi-neutrality, which indicates that around  $1-3 \text{ cm}^{-3}$  of electrons are not counted in this dataset.

To investigate the sensitivity of the following charging analysis to a missing population of electrons, intermediate results were computed with an added Maxwellian population with low density ( $10^{-5} \text{ cm}^{-3}$ ) and high temperature (200 keV) [29], as well as a dense ( $0.1 \text{ cm}^{-3}$ ) and cold (5 eV) population. The tenuous population makes no significant difference to the charging, but the dense and cold one does reduce the charging.

The statistical mean electron fluxes for GEO are shown in Fig. 2a, with the yellow sheet indicating  $K_P = 2-$  and the blue sheet for  $K_P = 8$ . For the calm condition, the flux monotonically decreases with energy and is fairly smooth with respect to local time. The storm flux is higher nearly everywhere and has a definite hump  $\sim 1 \text{ keV}$ , and a dramatic trough near local noon. There is also a lot more noisy texture with respect to local time.

The ion fluxes are shown with the same colors indicating the same  $K_P$  indices in Fig. 2b. The ion fluxes are more flat with respect to energy than the electron fluxes, but have a more distinct peak at low energy. Once again the storm flux is higher and more textured with respect to local time, although the low energy flux is lower during a storm except for a very sharp peak at local noon.

TABLE I: Space environment fits

	$n_E \text{ (cm}^{-3}\text{)}$	$T_E \text{ (keV)}$	$n_I \text{ (cm}^{-3}\text{)}$	$T_I \text{ (keV)}$
NASA worst case	1.1	12	0.24	29.5
ATS - 6	1.2, 1.2	16, 1	0.24, 0.00882	29.5, 0.111
Sept. 4	0.3, 0.2	4,7	0.3, 0.2	4,7

In the next row of plots, the electron and ion flux is compared to the single and Bi-Maxwellian fits used by NASCAP-2k [28] and shown in Tab. I. Fig. 2c shows the flux predicted by the three default options for electron flux at GEO alongside two traces from the empirical model - the upper one is chosen as a harsh charging condition ( $K_P = 8$ ,  $LT = 6$ ) and the lower one as a mild condition ( $K_P = 2-$ ,  $LT = 18$ ). The empirical model predicts significantly higher flux at low energies (which may be due to photoelectrons), similar flux at medium energies depending on the  $K_P$  and  $LT$ , and lower flux at higher energies above 10 keV than the Maxwellian fits.

For aluminum assuming isotropic electron flux, any flux between 120 eV and 6 keV produces more than one secondary electron and contributes to positive charging rather than negative charging. This "positive zone" is greyed out in the plot and sees more flux relative to the high energy zone above 6 keV in the empirical model than the Maxwellian models, which has implications for the net yields.

The empirical ion flux is compared to the same Maxwellian fits shown in Tab. I in Fig. 2d. The empirical trace with the large low energy spike corresponds to  $K_P = 8$ ,  $LT = 13$  and the other to  $K_P = 2-$ ,  $LT = 2$ . The empirical model predicts more flux everywhere than the Maxwellian models, especially at low energies. Additionally, the calm fluxes are much more flat in the empirical model. In the storm condition at local noon, there are two very distinct populations predicted by the empirical model, one with energy near 50 eV, and the other is much more spread out with an energy range of 1-20 keV.

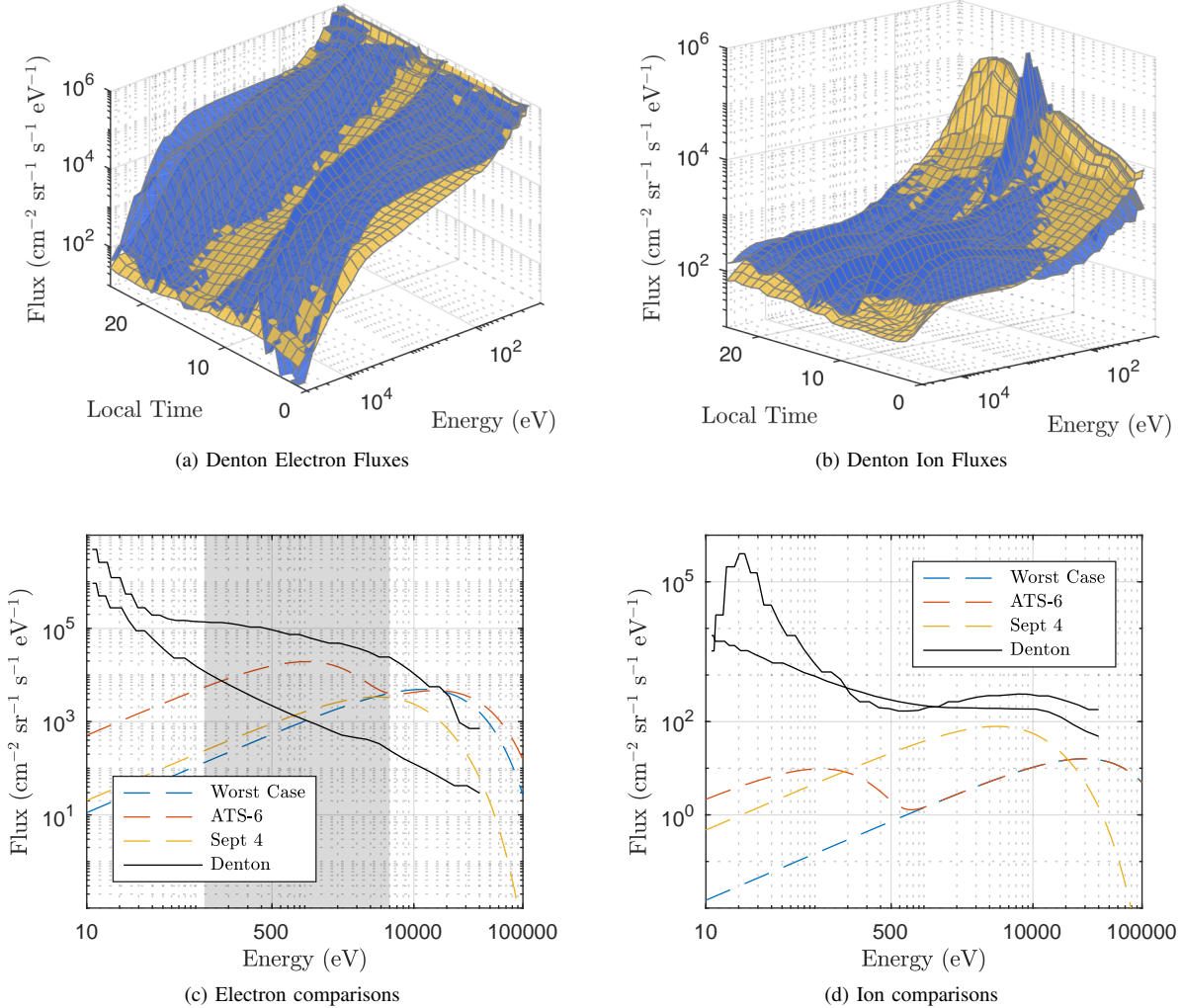


Fig. 2: Ion and electron fluxes at GEO for  $K_P = 2-$  (yellow) and  $K_P = 8$  (blue) as well as commonly used Maxwellian fits

A fundamental property of a Maxwellian fit when plotted on a log-log scale is its shape - It is always a hump with a shallow slope at low energies and steep slope at high energies. Changing the density moves it up and down, and changing the temperature moves it left and right, but neither of these properties change its width. Adding multiple Maxwellian populations with similar energy can approximate a wider peak, but there is no way to produce a narrow peak as is seen in the empirical storm flux at  $LT = 13$  using Maxwellian distributions.

### III. SPACECRAFT CHARGING

A space object is subject to many currents from the space plasma and the sun. The currents considered here are the thermal electron and ion currents ( $I_e$ ,  $I_i$ ), secondary electron emission (SEE) from both electrons and ions ( $I_{SEE_e}$ ,  $I_{SEE_i}$ ), electron backscattering ( $I_b$ ), the photoelectric current ( $I_{ph}$ ), and the beam current ( $I_{beam}$ ). The object is in equilibrium when the net current to it is zero:

$$I_e(\phi) + I_i(\phi) + I_{SEE_e}(\phi) + I_{SEE_i}(\phi) + I_b(\phi) + I_{ph}(\phi) + I_{beam}(\phi) = 0 \quad (1)$$

The charging model used in this analysis is based on that used in [30]. The main differences are that the beam current is included, the model for electron induced yields is changed to the NASCAP-2k model [31], and all yields other than that from the beam current assume isotropic flux rather than normal incidence. Brief explanations for the models for the various currents are presented next.

1) *Electron and Ion Thermal Currents*: Electrons and ions impact the spacecraft, electrons causing a negative current and ions stealing an electron and causing a positive current. For a flux distribution over energy  $F(E)$ , the current is

$$I(\phi) = q_0 2\pi A \int_L^\infty \left( \frac{E}{E \pm \phi} \right) F(E \pm \phi) dE \quad (2)$$

where  $q_0$  is the particle charge,  $A$  is the area exposed to the plasma, and  $\phi$  once again is the spacecraft potential. The lower bound of the integral  $L$  is 0 for the repelled particle, and  $|\phi|$  for the attracted particle. Ions take the upper sign and electrons take the lower.

Measured flux distributions are used and these integrals are done numerically using an adaptive quadrature integration program that uses linear interpolation on the flux data. The

flux data is logarithmically spaced in 40 increments for  $K_P = 2$ - and 50 increments for  $K_P = 8$  as shown in Figs. 2a and 2b. The lower bound for the attracted particle is  $|\phi| + 0.1$  V to avoid a mathematical singularity, and since data for  $F(E)$  only exists up to 40 keV for the distributions used, the upper bound is taken as  $40,000$  V +  $\phi$ . To counteract some of the enrichment of the low energy electron flux by photoelectrons and secondary electrons created on the spacecraft, the electron flux at all energies lower than 50 eV is reassigned to the flux at 50 eV.

2) *Secondary Electron Emission and Backscattering Current*: When an electron or ion impacts a material, it deposits much of its energy in the first few nanometers of the material. Some of this energy goes into freeing electrons near the surface which can escape the material. This phenomena is referred to as Secondary Electron Emission (SEE) and can significantly reduce the net electron thermal current and amplify the ion thermal current. Additionally, there is a chance that an electron bounces off the material rather than sticking. This phenomena is called “backscatter”. The probability that an electron backscatters is given by  $\eta$ , the expected number of secondary electrons generated by a single incident electron is typically given by  $\delta$ , and the total yield as  $Y = \eta + \delta$ . Since the total yield is a function of energy, it must be integrated over the distribution to find the current:

$$I(\phi) = q_0 2\pi A \int_L^\infty Y(E) \left( \frac{E}{E \pm \phi} \right) F(E \pm \phi) dE \quad (3)$$

Rather than calculating the actual current, the mean yield  $\langle Y \rangle$  is typically used which is the effective yield for a particular distribution.

$$\langle Y \rangle = \frac{I_Y}{I} = \frac{\int_L^\infty Y(E) \left( \frac{E}{E \pm \phi} \right) F(E \pm \phi) dE}{\int_L^\infty \left( \frac{E}{E \pm \phi} \right) F(E \pm \phi) dE} \quad (4)$$

The mean yield is a function of the distribution (which is a function of  $LT$ ), and the spacecraft voltage  $\phi$  which shifts the distribution. Once again, this integral is done numerically using the same adaptive quadrature integration program. The SEE function  $\delta$  for both ion and electron impact as well as the backscattering function  $\eta$  are discussed next.

The electron-induced SEE yield is typically small at low landing energies, then it rises to a large value for intermediate energies around a few hundred eV, then falls back to a small yield for keV energies. The NASCAP-2k model [31] for electron-generated SEE as a function of landing energy ( $E$ ) and angle ( $\psi$ ) is used with  $\psi = 0^\circ$  for the electron beam and a modification [32] to account for isotropic flux ( $\delta_I$ ) for the environmental currents:

$$\delta(E, \psi) = C \frac{1 - e^{-R\alpha \cos(\psi)} \sec(\psi)}{\alpha(b_1 q_1 E^{q_1-1} + b_2 q_2 E^{q_2-1})} \quad (5)$$

$$\delta_I(E) = 2CE \frac{R\alpha - 1 + e^{-R\alpha}}{(R\alpha)^2} \quad (6)$$

where  $R = b_1 E^{q_1} + b_2 E^{q_2}$  is the range of the electrons in the material. For Aluminum  $b_1 = 154 \text{ \AA}$ ,  $b_2 = 220 \text{ \AA}$ ,  $q_1 = 0.8$ , and  $q_2 = 1.76$ , assuming the landing energy  $E$  is in keV.

The parameters  $C$  and  $\alpha$  are hand tuned to  $C = 9.9808$ ,  $\alpha = 3.0486e8$  in order to match the peak yield and energy (for incident flux) of 0.97 and 400 eV.

3) *Electron backscattering*: Backscattering occurs when an electron is reflected from the spacecraft rather than absorbed. This analysis uses the model for energy-dependent backscattering provided in [31]. First the albedo for normal ( $A_N$ ) and isotropic ( $A_I$ ) flux are calculated:

$$A_N = 1 - (2/e)^{0.037Z} \quad (7)$$

$$A_I = 2 \frac{1 - \eta_0(1 - \log(\eta_0))}{\log(\eta_0)^2} \quad (8)$$

and then either are multiplied by a string of Heaviside step functions that account for low energy cases

$$\eta(E) = \left( \frac{H(1 - E)H(E - 0.05)\log\left(\frac{E}{0.05}\right) + H(E - 1)}{\log(20)} \right) \times \left( \frac{e^{-E/5}}{10} + A \right) \quad (9)$$

Where  $E$  is the landing energy in keV,  $H(x)$  is the Heaviside step function,  $\log$  is the logarithm with base 10, and  $Z$  is the atomic number of the material (aluminum in this analysis). The formulas above can be added to produce the total yield  $Y(E) = \eta(E) + \delta(E)$  for monoenergetic electrons.

Putting all of this together, the mean yield  $\langle Y \rangle$  is shown in Fig. 3 as a function of local time using the empirical model for flux as well as the three chosen Maxwellian fits for a spacecraft at 0 V.

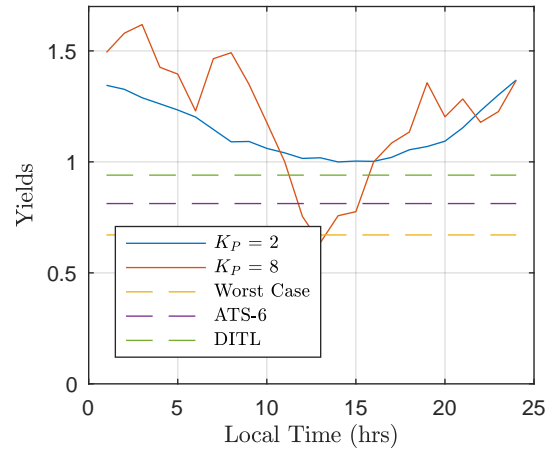


Fig. 3: Mean yields to an uncharged spacecraft using various environmental models

The yields computed using Denton’s model for flux are much higher than those from the Maxwellian distributions - this is due to the difference in flux in the “positive zone” from 120 eV and 6 keV. As a function of local time, the yield in both storm conditions dips near local noon, with it for  $K_P = 8$  actually dropping below 1 for a few hours. In all other conditions, the yield is larger than one, which means that the net electron current is positive, and no charging can occur.

In Reference [33], Ferguson et. al. propose that flux above 9 keV is the best proxy for charging, adding that charging will often occur if there is more than  $4e8$  electrons/cm<sup>2</sup>/s above 9 keV. The empirical model predicts flux higher than this threshold when  $K_P = 8$  at local times of 6 and 22 ( $12e8$  and  $11e8$  electrons/cm<sup>2</sup>/s of flux, respectively), but the isotropic aluminum yields for both of these instances are above 1, which prohibits any charging. This disagreement between the two models could be for many reasons. It is possible that averaging the flux misses some subtleties that affect the charging. For instance, a very hot but tenuous population one day and a very dense but cold population the next day will average to a flatter population and predict no charging on average, even though on the first day there would definitely have been charging.

Ions may also cause SEE, and for many materials the number of secondaries caused by ions is much larger than that caused by electrons. In this analysis the two parameter Nascap-2k model [31] for isotropic flux is used:

$$\delta(E) = 2 \frac{\beta E^{1/2}}{1 + E/E_M} \quad (10)$$

Where  $E$  is the energy in keV, and for aluminum  $\beta = 1.36$  and  $E_M = 40$  are fitting parameters. To get the mean yield, this function must be integrated alongside the ion flux as shown in Eq. (4).

4) *Photoelectric Current*: Energy from the sun can energize electrons in the first few nanometers of the spacecraft so that they leave the surface. The fraction that have enough energy to escape the potential well of the spacecraft cause a net positive current given by [34]:

$$I_p = \begin{cases} j_{ph} A e^{-q\phi/k_B T_{ph}} & \phi > 0 \\ j_{ph} A & \phi \leq 0 \end{cases} \quad (11)$$

Where  $j_{ph}$  is the photoelectron flux,  $A$  is the cross-sectional area, and  $k_B T_{ph}$  is the thermal energy of the ejected photoelectrons. For aluminum,  $k_B T_{ph} = 2$  eV and  $j_{ph} = 40$   $\mu\text{A}/\text{m}^2$ . For a negative spacecraft this current is constant, and for a positive spacecraft it quickly vanishes.

5) *Beam Current*: The electron beam will only escape the potential well of the tug and cause any charging if it has sufficient energy. If it has enough energy to escape the well of the tug, but not to reach the debris, it will deflect and fly off into space and cause a net current on the tug but not the debris. Finally, if the beam is energetic enough it will reach the debris and cause a negative current. The yield for the electron beam is calculated assuming normal incidence and from the landing energy  $LE = q_0(V_b - \phi_T + \phi_D)$  where  $V_b$  is the accelerating voltage of the beam, and  $\phi_T$  and  $\phi_D$  are the potentials of the tug and debris respectively. In reality, the debris may be rotating so the angle of incidence will change as the angle between the beam and the debris surface changes, which will reduce the effectiveness of the beam.

#### A. Equilibrium Voltage

For the spacecraft to be in equilibrium with its environment, it must assume the voltage that causes no net current. This is done numerically by root solving Eq. (1) for different

local times and different net beam current densities. The beam current density is computed as the actual beam current (which would be directed in a small spot) divided by the total surface area of the spacecraft. For the debris, this current must be reduced using the yield. The photoelectric current is only applied on 1/4 of the total surface area, since the cross sectional area of a sphere is 1/4 the total area. This normalization allows the spacecraft charging calculations to be done once and then interpolated to cover a wide variety of cases. These voltages are shown in Fig. 4.

The top plot (Fig. 4a) shows the equilibrium voltage at  $K_P = 2$ — computed using the empirical model. The upper sheet represents the tug for which the beam is a positive net current, and the lower sheet represents the debris for which the beam is negative. The most obvious trend is that it takes less beam current to charge negative than positive. Next, at low beam currents it is very hard to charge negative. This is because the photoelectron current very effectively resists any negative charging until it is overwhelmed by the beam. It is easiest for the tug to charge positive in the late night sector, and easiest for the debris to charge negative near local midnight.

The middle plot (Fig. 4b) shows the tug and debris equilibrium voltages in the same format, but for  $K_P = 8$ . There is a lot more variation over local time during a storm - the tug can charge positive very easily near local noon and has a difficult time everywhere else. The debris has a much more complex trend across local time, but it experiences both more and less charging than the calm case at different local times.

The bottom plot (Fig. 4c) compares the equilibrium voltage found the empirical model with that from using the Sept. 4 Bi-Maxwellian fit, a single Maxwellian fit used in prior charging analysis of the ET, and the SCATHA data. The empirical voltages are shown as colored blocks that encompass the curves at all local times with yellow and blue representing the calm and stormy condition. The increased variation over local time at  $K_P = 8$  can clearly be seen in this format. The Sept. 4 model uses the Bi-Maxwellian fit presented in Tab. I and predicts more positive charging than the empirical model at either storm condition at high currents. It also predicts a much more negative voltages for the debris once the current overpowers the photoelectron current ( $10 \mu\text{A}/\text{m}^2 = j_{ph}/4$ ). This is because the ion populations are very hot which reduces the ion current significantly. The fit from prior work uses the parameters from Hogan and Schaub [22] and due to the much lower ion temperature it predicts a less extreme voltage for the debris past the photoelectric cutoff. The SCATHA data is taken from [35] where the spacecraft emitted a electron beam and charged itself up to 3 keV. Since the charging was often limited by the energy of the beam, the spacecraft voltage at that beam current might be even higher if the beam energy was increased. The surface area of SCATHA, if approximated by a cylinder, is  $13.5 \text{ m}^2$  [36]. SCATHA is made from many different materials with different SEE parameters and is also spinning which changes the sunlit area as a function of time, thus, these data points are provided more as an order of magnitude estimate.

The charging models based on Maxwellian flux, empirical flux, and the SCATHA data all have sources of error. For the purposes of the ET, which takes a few months to tow a debris

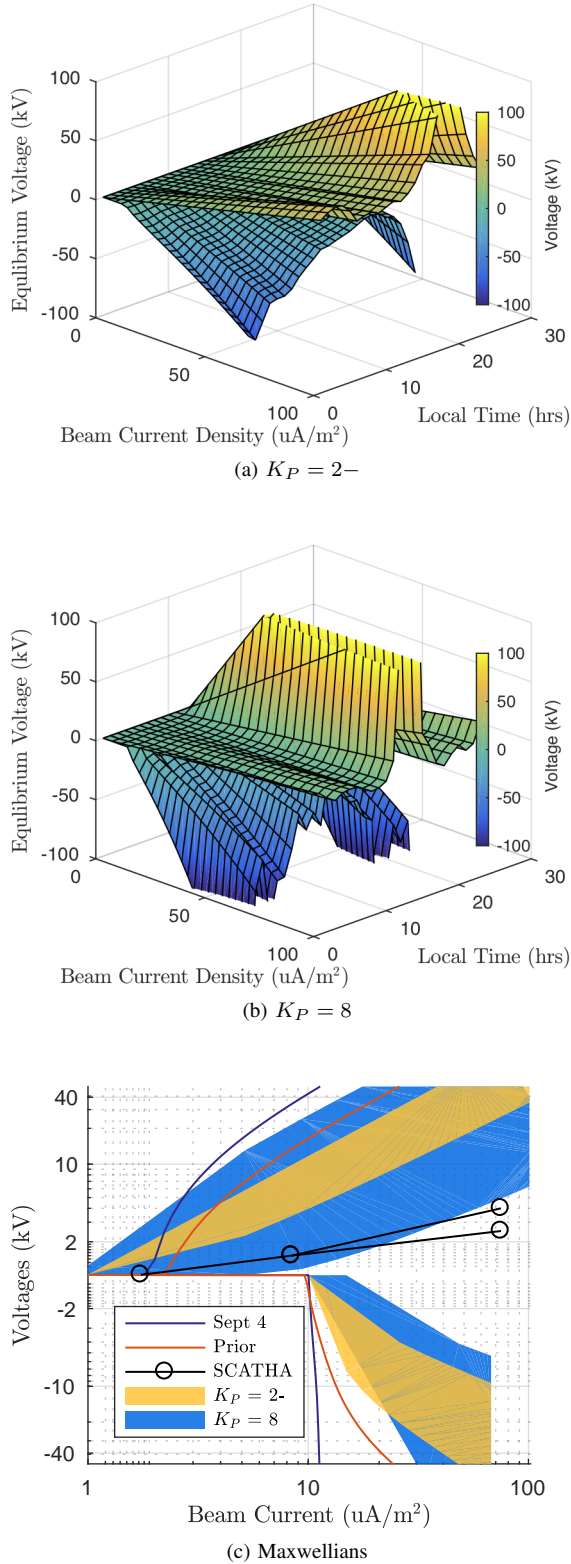


Fig. 4: Equilibrium voltages for tug and debris at different local times and beam currents

object out of GEO, the empirical flux data changing model is used because it provides a better estimate of the average space weather that would be encountered on such a multi-month trip. It is worth noting that all three classes of models predict similar trends in performance.

#### IV. FORCE ANALYSIS

To find the force between two spacecraft, the tug and debris radius must be chosen along with the beam current and energy. Using the tug radius and beam current along with local time, the tug potential can be found by directly interpolating the top sheet of Fig. 4. Finding the debris potential is unfortunately more difficult. The yield from the electron beam reduces the net current and is a function of the landing energy of the beam. Thus, to find the net electron beam current and interpolate the debris potential, one would need to already know the debris potential in order to compute the yield. To solve this problem, a function is written which takes a candidate debris voltage, then computes the actual beam current as well as the needed beam current to support that voltage. The debris voltage is varied so that these two numbers are identical. Using this procedure, the equilibrium voltages of two spacecraft can be found easily as a function of their sizes, beam energy and current, and the local time.

Once the voltages are known, they must be transformed to charges to compute the force. The charges are related to the voltages through an elastance matrix:

$$\begin{bmatrix} V_T \\ V_D \end{bmatrix} = \begin{bmatrix} 1/R_T & 1/\rho \\ 1/\rho & 1/R_D \end{bmatrix} \begin{bmatrix} Q_T \\ Q_D \end{bmatrix} \quad (12)$$

Then, the force is computed with Coulomb's force law:

$$F = \frac{Q_T Q_D}{4\pi\epsilon_0\rho^2} \quad (13)$$

A sheath will form around both spacecraft which will reduce the force between them, but it is ignored in this analysis. Prior work [37] has shown that it is very small, typically less than 1%, for the small separations considered here.

Consider the example case of a 3 m tug and a 2 m debris separated by  $\rho = 4(R_T + R_D) = 20$  m. The attractive force between them is shown in Fig. 5 at  $K_P = 2-$  and  $K_P = 8$ . The force generally increases with a higher voltage and current, and has a decent amount of texture with respect to local time. The highest force is near local midnight for the calm space weather condition when it is easiest for the debris to charge very negative. The force grows quickly with current when the current is low, but seems to saturate at higher currents. During storm time there is a lot more variation in force throughout the orbit, and the force actually decreases with current for some local times.

#### V. AVERAGE FORCE ANALYSIS

The total re-orbiting time will be better related the orbit-averaged force than the instantaneous force. The orbit averaged force is computed by averaging the forces across local time. These forces are shown in Fig. 6 for a 20, 40, 60, and 80 kV beam assuming the same 3 m tug and 2 m debris separated

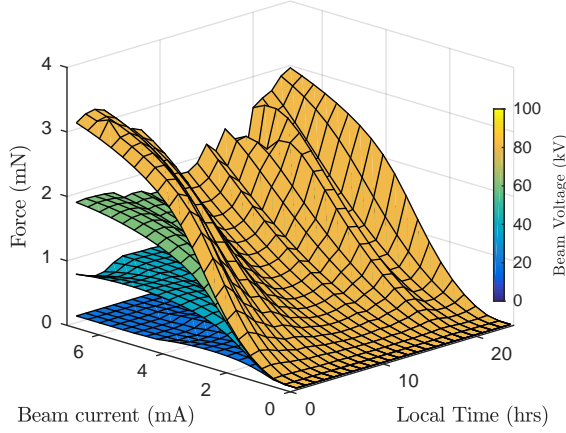
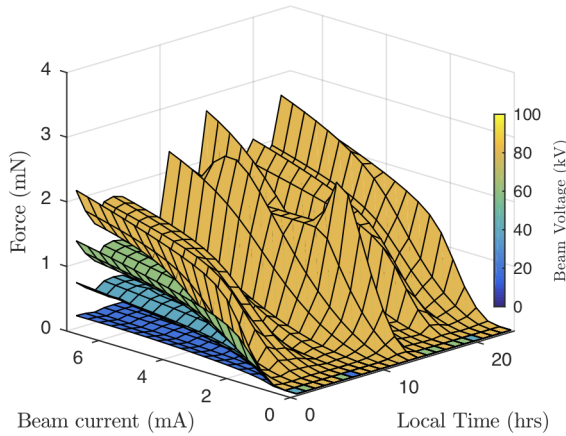
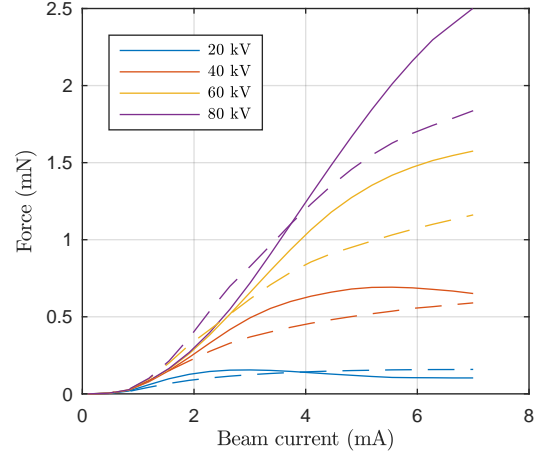

 (a)  $K_P = 2-$ 

 (b)  $K_P = 8$ 

Fig. 5: Force between a 3 m tug and 2 m debris separated by 20 m as a function of beam current, voltage, and local time

by 20 m. The continuous lines represent  $K_P = 2-$  and the dashed lines represent  $K_P = 8$ .

The 20 kV beam performs just as well as the higher energy beams until about 1 mA where the higher energy beams split. The 40 kV beam stays with the others until about 2 mA, and the 60 kV stays with the 80 kV until 3 mA. The reason for this behavior is that the extra beam voltage doesn't really help until the debris and tug are charged so differently that the extra accelerating voltage is needed for the beam to reach the debris. These departure currents must be the currents at which the potential difference between the two craft is either 40, 60, or 80 kV. The SEE current is also a function of the landing energy, which is why the curves aren't quite identical below the departure currents.

The orbit averaged storm forces are slightly lower than the calm forces except for low current for the 80 kV beam and high current for the 20 kV beam. This differs from prior work [22, 26] which always found higher forces during a storm. This difference is due to the very different charging


 Fig. 6: Orbit averaged force as a function of beam current, voltage, and local time. Dashed lines represent  $K_P = 8$ , and continuous lines represent  $K_P = 2-$ 

and environmental models used, which only share the model for the photoelectric current.

## VI. RELATIVE SIZING ANALYSIS

In prior work, Hogan et al [38] found that small tug vehicles would have a hard time charging a much larger debris object. This is because while for the small tug the beam current is enough to cause significant charging, it will barely overcome the photoelectric current on the large debris. This analysis is repeated here, but from a force rather than charging perspective. Because of the induced charge, there is an attractive force even if there is no change in the debris voltage. The force as a function of beam power between a 3 m tug and different debris sizes is shown in Fig. 7a. The separation distance for all cases is 20 m.

The maximum force is found as a function of power for a variety of different debris sizes - the tug size is fixed at 3 m so the ratio of tug to debris radius spans from 0.5 up to almost 2. The force is very linear with power with a slope of roughly 1/2 a mN per 100 Watts of power regardless of debris size. Because it is difficult to see departures from this trend at this scale, the difference in force from this linear fit is shown in in Fig. 7b. The highest force (or least negative in this plot) is when  $R_D = R_T = 3$  m at most powers with  $R_D = 2$  and 4 m very near. The extreme ends of the spectrum where  $R_D$  is 1.5 or 5 meters produce less force. This is because the beam can be close to optimal for both craft when they are the same size, but not when they are different sizes.

## VII. PULSING ANALYSIS

Prior work has considered a pulsed electron beam rather a constant-current beam [25, 26]. The benefits to pulsing are twofold - first it introduces windows where both spacecraft are discharged and the beam is off which can be used for communications, thrusting, or measurements to be taken that might be interfered with by the beam. Secondly, pulsing the beam can increase the force at a given power level. To motivate

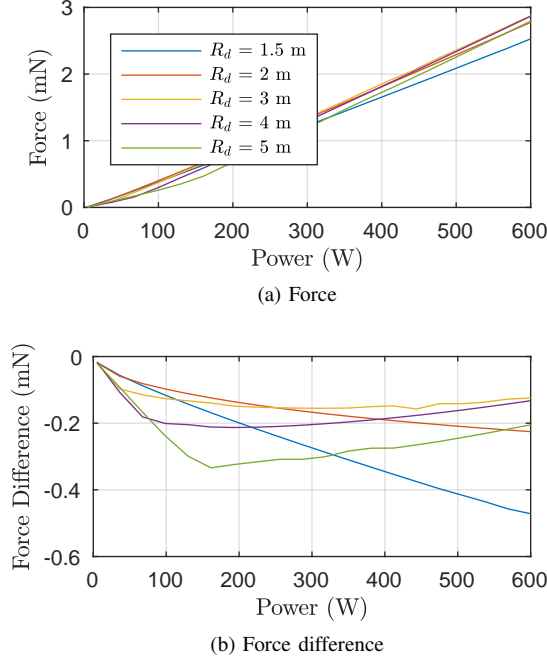


Fig. 7: Best possible force at different powers for different tug to debris size ratios at  $K_P = 2-$

this phenomena consider two electron beams, one with energy of 10 keV continuously operating and one with 20 keV of energy on for half the time. Further assume that the current for both beams is the same so that they have the same average power. The 10 keV beam would charge the tug and debris to 5 keV and -5 keV and hold them there, while the pulsed beam could charge the tug and debris to  $\pm 10$  keV when the beam is on and 0 V when it is off. If mutual capacitance is ignored, the pulsed tug and debris charges will both double the continuous case during the time that the beam is on. Since the force is proportional to the product of the charges, the pulsed case will have 4 times the force when the beam is on, and zero when it is off. This amounts to the average pulsed force being double that of its continuous counterpart. Of course, the current must also be raised so the voltage cannot quite double, and there are a few other effects that limit the force increase.

In this analysis, the optimal force at different power levels shown in Fig. 7 will be re-used. If the pulse period is large compared to the charge up time, the force that a pulsed beam produces can be approximated as the equilibrium force for the duration of the pulse period. Since the capacitance of the objects considered here are around  $4\pi\epsilon_0 R \approx 10^{-10}$  Farads, a 1 mA beam could change the voltage by 1 kV in approximately 0.1 ms, this assumption of steady state forces will be valid for all pulse periods larger than 1 second.

With this assumption the charge-up and charge-down behavior is ignored and the average force produced by a pulsed beam is given by

$$F_P(P, d) = d F_M(P/d) \quad (14)$$

where  $F_M(x)$  is the maximum force at a power level of  $x$ ,  $F_P$  is the average force from a pulsed beam at power  $P$  with

a duty cycle of  $d$ , which is the fraction of time that the beam is on. During the “on” part of the cycle, the power can be raised to  $P/d$  without changing the average power since it is not operating while the beam is off. Multiplying the force by  $d$  accounts for it being on only  $d$  of the time.

If the maximum force is directly proportional to power, there is no benefit at all to pulsing because the  $d$ s would cancel each other out. However, if the force increases quadratically, or is linear with an offset, there can be an increase in force. The increase in force from moving from a continuous beam to a pulsed beam of the same power is shown in Fig. 8 for the case of the tug and debris both having a radius of 3 m.

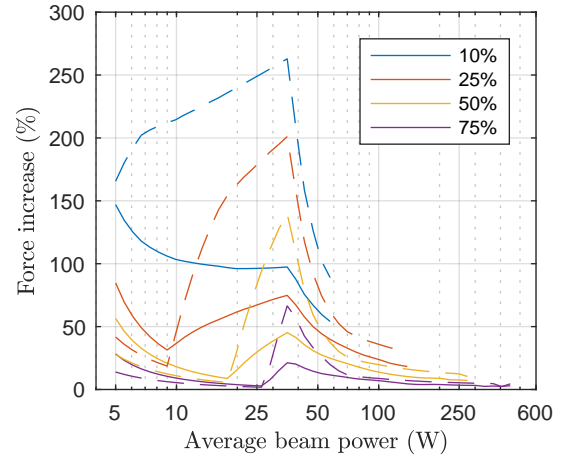


Fig. 8: Force increase as a function of duty cycle and power. Continuous lines represent  $K_P = 2-$  and dashed lines represent  $K_P = 8$ .

A pulsed beam almost always increases the force for a given power level, with the largest gains found for low power and low duty cycles. For very low powers, the pulsed force can be more than 2 times larger than the continuous force, and even at 100 W a pulsed beam can improve the force by 25%. Because the max beam voltage is set at 100 kV, the low duty cycle beams are infeasible at high power levels because they require too high of a beam voltage while the beam is on. The increases are larger during stormy conditions especially near 25 Watts.

Now consider varying the tug to debris size ratio as well as pulsing. Referring again to Fig. 7, the force is more convex when the debris is larger than the tug. This would indicate that pulsing would be more advantageous when the tug is smaller than the debris since the gain from the force at the higher power level  $F_M(P/d)$  would outweigh the loss from only being on  $d$  of the time. The ratio of the pulsed to continuous force is shown below in Fig. 9

The force ratio is shown for the power levels of 25 W (continuous lines), 50 W (dashed lines), and 100 W (dots). The lines end at low duty cycles when the beam voltage required is larger than 100 kV, which happens sooner for the high power cases than the low power ones. The force ratio is by definition 1 at a 100% duty cycle, and either increases or decreases for different debris sizes. All debris sizes benefit from pulsing at

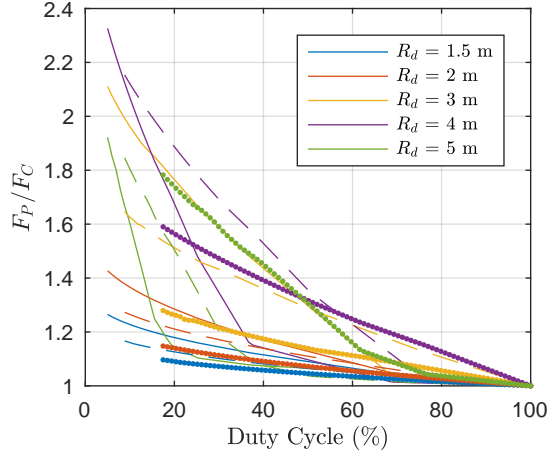


Fig. 9: Force ratio as a function of tug and debris sizes and duty cycle at  $K_P = 2$ — with continuous lines representing 25 W, dashed lines representing 50 W, and dots representing 100 W of power.

these power levels, but the biggest gains are for the larger debris (green and purple lines). The smallest debris object additionally start to trend downward for very low duty cycles.

### VIII. ORBIT RAISING

If the forces as a function of local time are used as a purely along-track acceleration in Gauss' variational equations, the change in the orbit can be found. The acceleration is found by estimating the mass from the relationship originally presented in [11] and dividing to find the acceleration.

$$M(\text{kg}) = 1507(R(m) - 1.152) \quad (15)$$

First the semi-major axis (SMA) change per orbit equation [11] for a purely along track acceleration is

$$\Delta a = \frac{4\pi F}{n^2 m} \quad (16)$$

where  $n$  is the mean motion of the orbit. Then, for each debris radius and power level, calculate the time it would take to raise the SMA by 250 km using the mean motion at its initial orbit radius. This is shown in Fig. 10. In general using more power reduces the time it takes to move the debris to the graveyard orbit, but the gains are greater at lower powers. It takes the 3 m tug a little more than 3 months to tug another 3 m object to the graveyard orbit. In contrast it only takes 22 days if tugging a 1.5 m debris, and 7 months if tugging a 5 m object. Clearly the ratio between the debris and tug sizes is very important for tugging. Keeping in mind that the tug size is purely for self capacitance and current collection; with sufficiently large deployable structures, the tug could be a lightweight cubesat.

Next, consider a higher fidelity orbital analysis but only for one scenario. The rates of the classical orbit elements are found due to the acceleration which changes with local time and integrated with an RK4 integrator. The only rates of interest that have a sensitivity to an along track acceleration are the semi-major axis, the eccentricity, and the argument of perigee.

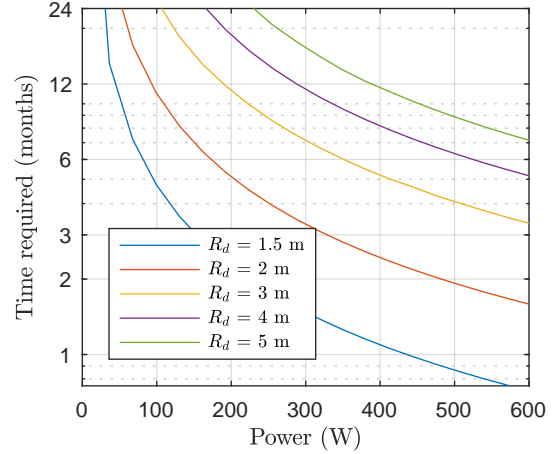


Fig. 10: Time to move GEO debris to a graveyard orbit for a 3 m tug

This analysis can show how long it will take a tractor to pull a debris object into the graveyard orbit, and also what happens to the other orbital parameters during this operation. Consider a 3 meter tug and 2 m debris object separated by 20 m at nominal altitude inclined by  $1^\circ$ . The change in the perigee radius is shown in Fig. 11. The perigee radius is shown rather than the semi-major axis because that is the parameter that needs to be increased in order to prevent future collisions.

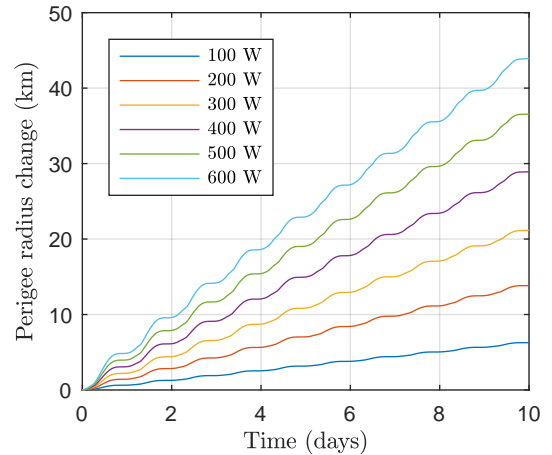


Fig. 11: Change in perigee radius over 1 week of operation

If the tractor can use 600 Watts of power, it can tug this debris object into the graveyard orbit in 57 days using this average rate. The beam voltage required is 77 kV and the current is 7.8 mA. If it can only use 100 W of power it will take 398 days, or 13 months. These estimates predict slightly larger times to the graveyard orbit than Fig. 10, but are still in the same ballpark. This is expected since the analytical method does not account for the changing eccentricity or the coupled nature of the rates.

## IX. CONCLUSIONS

A new charging model for the Electrostatic Tractor (ET) is developed which uses an empirical model for the electron and ion fluxes which is used to compute the thermal electron and ion currents as well as the SEE and backscattering yields as well as accounting for isotropic incidence in the yields. The major impact of this new model relative to prior work is that it is much harder for an object to charge negative due to the higher yields. This model is used to predict the forces for a variety of beam currents and voltage as well as tug and debris sizes at both  $K_P = 2-$  and  $K_P = 8$ . It is found that the force is highest near local midnight, and that the orbit averaged forces only depend on the beam voltage past a current threshold. The forces are mostly linear with power with a slope of around 1/2 a mN per 100 Watts for a 3 m tug

Pulsing is the most effective for large debris objects at low powers, but pulsing still provides force increases for all scenarios evaluated as well as opening windows for controls and sensing to take place without interference from the beam. Orbit raising is considered next, the ET is most effective when tugging small debris, but that is only because they are assumed to be light. A tug spacecraft could also deploy large conducting surfaces to increase its effective radius without significantly changing its mass. For many scenarios, a tug could pull a debris object from the operational GEO ring to a graveyard orbit in a few months. Overall, the higher fidelity charging model finds that more current and power is required to operate the ET but it is still a feasible mission concept for touchlessly tugging space debris to the graveyard orbit.

## REFERENCES

- [1] B. Streetman and M. A. Peck, "New synchronous orbits using the geomagnetic lorentz force," *AIAA Journal of Guidance, Control, and Dynamics*, vol. 30, no. 6, pp. 1677–1690, Nov.–Dec. 2007.
- [2] B. Streetmann and M. A. Peck, "Gravity-assist maneuvers augmented by the lorentz force," *Journal of Guidance, Control, and Dynamics*, vol. 32, no. 5, October 2009.
- [3] Y. Yan, X. Huang, and Y. Yang, *Dynamics and Control of Lorentz-Augmented Spacecraft Relative Motion*. Springer, 2017.
- [4] J. Berryman and H. Schaub, "Analytical charge analysis for 2- and 3-craft coulomb formations," *AIAA Journal of Guidance, Control, and Dynamics*, vol. 30, no. 6, pp. 1701–1710, Nov.–Dec. 2007.
- [5] E. Hogan and H. Schaub, "Collinear invariant shapes for three-craft coulomb formations," *Acta Astronautica*, vol. 12, pp. 78–89, March–April 2012.
- [6] P. D. Jasch, E. A. Hogan, and H. Schaub, "Out-of-plane stability analysis of collinear spinning three-craft coulomb formations," *Acta Astronautica*, vol. 88, pp. 89–97, July–Aug. 2012.
- [7] L. B. King, G. G. Parker, S. Deshmukh, and J.-H. Chong, "Study of interspacecraft coulomb forces and implications for formation flying," *AIAA Journal of Propulsion and Power*, vol. 19, no. 3, pp. 497–505, May–June 2003.
- [8] T. Bennett, D. Stevenson, E. Hogan, L. McManus, and H. Schaub, "Prospects and challenges of touchless debris despinning using electrostatics," *Advances in Space Research*, vol. 56, no. 3, pp. 557–568, 2015.
- [9] T. Bennett and H. Schaub, "Touchless electrostatic three-dimensional detumbling of large axi-symmetric debris," *Journal of Astronautical Sciences*, vol. 62, no. 3, pp. 233–253, 2015.
- [10] D. Stevenson and H. Schaub, "Rotational testbed for coulomb induced spacecraft attitude control," in *5th International Conference on Spacecraft Formation Flying Missions and Technologies*, Munich, Germany, May 29–31 2013.
- [11] H. Schaub and L. E. Z. Jasper, "Orbit boosting maneuvers for two-craft coulomb formations," *AIAA Journal of Guidance, Control, and Dynamics*, vol. 36, no. 1, pp. 74–82, Jan. – Feb. 2013.
- [12] H. Schaub and D. F. Moorero, "Geosynchronous large debris reorbiter: Challenges and prospects," *The Journal of the Astronautical Sciences*, vol. 59, no. 1–2, pp. 161–176, 2014.
- [13] D. J. Kessler and B. G. Cour-Palais, "Collision frequency of artificial satellites: The creation of a debris belt," *Journal of Geophysical Research*, vol. 83, no. A6, pp. 2637–2646, Jun. 1978.
- [14] D. Oltrogge and T. Kelso, "Getting to know our space population from the public catalog," in *Astrodynamic Specialist Conference, Girdwood, AK, USA*, 2011.
- [15] P. V. Anderson and H. Schaub, "Local orbital debris flux study in the geostationary ring," *Advances in Space Research*, vol. 51, no. 12, pp. 2195–2206, 2013. [Online]. Available: <http://www.sciencedirect.com/science/article/pii/S0273117713000410>
- [16] —, "Local debris congestion in the geosynchronous environment with population augmentation," *Acta Astronautica*, vol. 94, no. 2, pp. 619–628, Feb., 2014.
- [17] D. S. McKnight and F. R. D. Pentino, "New insights on the orbital debris collision hazard at geo," *Acta Astronautica*, vol. 85, pp. 73–82, April–May 2013. [Online]. Available: <http://www.sciencedirect.com/science/article/pii/S0094576512004869>
- [18] D. McKnight, "Pay me now or pay me more later: start the development of active orbital debris removal now," in *advanced Maui optical and space surveillance technologies conference*, 2010.
- [19] P. Chrystal, D. McKnight, P. L. Meredith, J. Schmidt, M. Fok, and C. Wetton, "Space debris: On collision course for insurers?" Swiss Reinsurance Company Ltd, Zürich, Switzerland, Tech. Rep. 1504360-11-en, March 2011.
- [20] D. L. Oltrogge, S. Alfano, C. Law, A. Cacioni, and T. S. Kelso, "A comprehensive assessment of collision likelihood in geosynchronous earth orbit," in *International Astronautical Congress*, Adelaide, Australia, Sept. 25–29 2017.
- [21] H. Schaub and Z. Sternovsky, "Active space debris charging for contactless electrostatic disposal maneuvers," *Advances in Space Research*, vol. 53, pp. 110–118, 2013.

- [22] E. A. Hogan and H. Schaub, "Impacts of hot space plasma and ion beam emission on electrostatic tractor performance," *IEEE Transactions on Plasma Science*, vol. 43, no. 9, pp. 3115–3129, 2014.
- [23] E. Hogan and H. Schaub, "Space weather influence on relative motion control using the touchless electrostatic tractor," *Journal of Astronautical Sciences*, vol. 63, no. 3, pp. 237–262, 2016.
- [24] M. H. Denton, M. F. Thomsen, H. Korth, S. Lynch, J. C. Zhang, and M. W. Liemohn, "Bulk plasma properties at geosynchronous orbit," *Journal of Geophysical Research*, vol. 110, no. A7, July 2005. [Online]. Available: <http://dx.doi.org/10.1029/2004JA010861>
- [25] J. Hughes and H. Schaub, "Prospects of using a pulsed electrostatic tractor with nominal geosynchronous conditions," *IEEE Transactions on Plasma Science*, vol. 45, no. 8, pp. 1887–1897, 2017.
- [26] —, "Orbital and storm time analysis of the pulsed electrostatic tractor," in *European Conference on Space Debris*, ESOC, Darmstadt, Germany, April 18 – 21 2017.
- [27] M. Denton, M. Thompson, V. Jordanova, M. Henderson, J. Borovsky, J. Denton, D. Pitchford, and D. Hartley, "An empirical model of electron and ion fluxes derived from observations at geosynchronous orbit," *AGU Space Weather*, vol. 13, pp. 233–249, 2015.
- [28] V. Davis, B. Gardner, M. Mandell, and K. Wilcox, *NASCAP-2k User's Manual*, 4th ed., Science Applications International Corporation, San Diego, CA 92121, February 2011.
- [29] J. E. Borovsky, T. E. Cayton, M. H. Denton, R. D. Belian, R. A. Christensen, and J. C. Ingraham, "The proton and electron radiation belts at geosynchronous orbit: Statistics and behavior during high-speed stream-driven storms," *Journal of Geophysical Research: Space Physics*, vol. 121, 2016.
- [30] J. Hughes and H. Schaub, "Effects of space weather on geosynchronous electromagnetic spacecraft perturbations using statistical fluxes," in *AGU Fall Meeting*, New Orleans, LA, Dec 11 – 15 2017.
- [31] V. Davis and M. J. Mandell, *Plasma Interactions with Spacecraft. Volume 2, NASCAP-2K Scientific Documentation for Version 4.1*, 4th ed., Science Applications International Corp, 2011.
- [32] I. Katz, D. E. Parks, M. Mandell, J. M. Harvey, D. H. Brownell, S. Wang, and M. Rotenberg, "A three dimensional dynamic study of electrostatic charging in materials," Systems, Science, and Software, Tech. Rep., 1977.
- [33] D. Ferguson, R. Hilmer, and V. Davis, "Best geosynchronous earth orbit daytime spacecraft charging index," *Journal of Spacecraft and Rockets*, vol. 52, no. 2, 2015.
- [34] S. T. Lai, *Fundamentals of Spacecraft Charging: Spacecraft Interactions with Space Plasmas*. Princeton University Press, 2011.
- [35] M. Gussenhoven, E. Mullen, and D. Hardy, "Artificial charging of spacecraft due to electron beam emission," *IEEE Transactions on Nuclear Science*, vol. NS-34, no. 6, 1987.
- [36] G. W. Schnueller, M. J. Mandell, D. E. Parks, P. G. Steen, J. J. Cassidey, I. Katz, and A. Rubin, "Charging analysis of the scatha satellite," Air Force Geophysics Laboratory, Tech. Rep. NAS3-21050, 1979.
- [37] C. R. Seubert, L. A. Stiles, and H. Schaub, "Effective coulomb force modeling for spacecraft in earth orbit plasmas," *Advances in Space Research*, 2014.
- [38] E. A. Hogan, "Impacts of tug and debris sizes on electrostatic tractor charging performance," *Advances in Space Research*, vol. 55, no. 2, pp. 630–638, Jan 2014.